The Pattern Selection Capability of a Printed ESPAR Antenna

Leonidas Marantis[1], Konstantinos Maliatsos[1], Christos Oikonomopoulos-Zachos[2], Dimitrios K. Rongas[1], Anastasios Paraskevopoulos[1], Antonios Aspreas[1], Athanasios G. Kanatas[1]
[1] University of Piraeus, School of ICT, Department of Digital Systems, Piraeus, Greece, leomarantis@unipi.gr
[2] IMST GmbH, Antennas & EM Modelling, Kamp-Lintfort, Germany, oikonomopoulos@imst.de

***Abstract*—The research work presented in this paper involves a proof-of-concept indoor experiment that demonstrates the beamforming capability of an Electronically Switched Parasitic Array Radiator (ESPAR) antenna. A new 3-element ESPAR antenna, formed by one active and two parasitic printed monopoles, is proposed. Two prototypes, which operate at 3.55 GHz, are modeled, fabricated and measured, exhibiting a reconfigurable pattern (three operating modes) and a satisfying directivity increase between the omni-directional and the two directional states. The two ESPARs are embedded in a IEEE 802.11p transceiver, in order to perform a beam selection concept in an indoor environment and evaluate the overall performance in a system level. When the two antennas focus their radiations patterns towards each other, an average of more than 6.5 dB Signal to Noise Ratio (SNR) gain is achieved, compared to the omnidirectional mode.**

***Index Terms*—ESPAR, pattern selection, beamforming, printed monopole, reconfigurable antenna.**

I. Introduction

The various performance restrictions that can be imposed by the propagation environment in wireless communications, have given rise to new antenna technologies. Smart antennas that are able to exhibit a reconfigurable radiation pattern can be regarded as one of the most prosperous fields in antenna engineering [1]. Reconfigurable pattern antennas can enhance the performance of a wireless system, decrease interference and offer re-use of channels (by neighboring users). Moreover, in vehicular or mobile applications, where the antenna needs to be installed in rather small spaces (e.g. side mirrors) or in compact handheld terminals, the dimensions of the antenna possess a crucial role [1].

The ESPAR antenna [2]-[4] can be considered as an excellent candidate to fulfill the pattern reconfigurability requirement (and various other features of a MIMO system [5]). At the same time, it provides comparably small dimensions and it maintains a low complexity and a low cost design (single RF chain), since the parasitic elements do not involve complex feeding and control circuits.

Section II presents a new printed ESPAR antenna design along with the simulation results. Section III includes the fabrication details of the two prototypes and the S_{11} and radiation pattern measurement results. Measured return loss and far-field patterns demonstrate a good agreement with the design. In Section IV, the proof-of-concept indoor experiment is demonstrated along with the SNR comparison results. A series of indoor measurement tests were held in the University of Piraeus premises in order to demonstrate the beamforming advantage of the antenna and evaluate the enhancement of a IEEE 802.11p system. The obtained results prove that the proposed ESPAR equipped system achieves a significant SNR increase. Section V provides the final conclusions of the investigation.

II. Configuration of the Printed ESPAR Antenna and the Simulation Results

A. ESPAR Antenna Design

The ESPAR antenna model is designed in the CST 3D electro-magnetic simulator [6]. The detailed layout of the antenna is presented in Fig. 1, along with the basic parameterized dimensions of the structure. The proposed ESPAR consists of three elements (one active printed monopole and two parasitic printed monopoles). A RO-4725 JXR (57 x 40 mm) dielectric substrate (h = 0.78 mm, ε_r = 2.55), purchased from Rogers Corporation, is employed in order to "accommodate" the antenna elements along with the controlling circuit. The active printed antenna element is composed by an end-launch (edge-fed) SMA connector, a microstrip quarter wavelength transformer (to convert the 50 Ω impedance to the theoretical 37 Ω input impedance) and the printed λ/4 monopole.

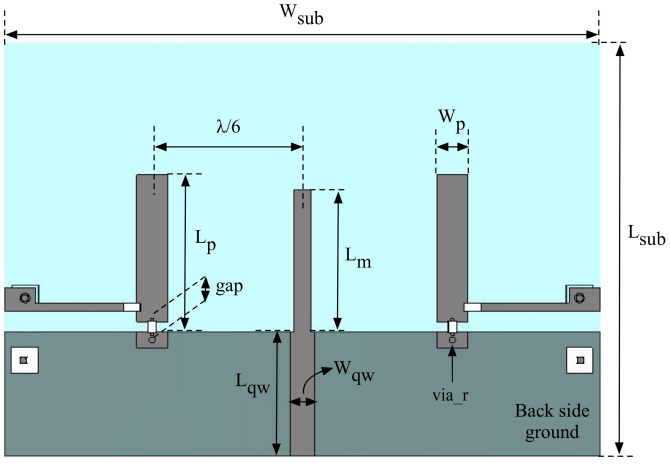

Fig. 1. The "top-view" layout of the ESPAR simulation model in CST. The ground plane stripe (printed at the back side of the panel) is also visible since the substrate is left out of the diagram.

The dielectric panel is excluded from the illustration in order to make the ground plane at the back side visible. Beamforming is implemented by allocating two parasitic printed monopoles next to the active element (one at each side), in a relatively short distance (λ/6). Strong mutual coupling is induced and radiation pattern reconfigurability is achieved by employing two PIN diode electronic switches (with two operation states – ON or OFF) in order to control which parasitic element is grounded. The monopole is connected to the ground plane stripe by a platted via, forming an L-shaped reflector that focuses the antenna beam to the opposite direction. Fig. 2 demonstrates the two equivalent circuits that are employed in order to simulate the two PIN diode states.

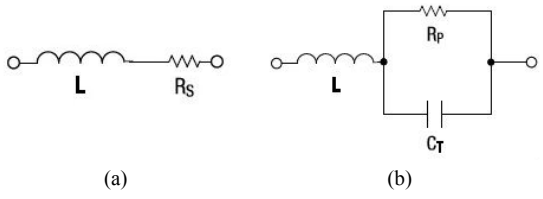

Fig. 2. The two equivalent circuits for the (a) ON (R_s = 0.9 Ω, L = 0.45 nH) and the (b) OFF (C_T = 0.3 pF, R_p = 1 KΩ) state of the diode switch.

The number of possible pattern combinations is four. However, the ON-ON operating mode is excluded since it does not provide a satisfactory return loss response for the desired frequency of 3.55 GHz, ending up with three feasible pattern states (OFF-OFF, ON-OFF, OFF-ON). The antenna design also includes a two-branch DC bias network that is necessary in order to apply voltage to the two PIN diodes and change their operating mode. Two RF chokes are also realized by two chip inductors that are located at the start of the DC bias lines. The basic dimensions of the antenna design are given in Table I in mm.

TABLE I. ESPAR ANTENNA DIMENSIONS

Parameter	***Description***	***Value (mm)***
t	thickness of the copper and the ground plane layers	0.035
L_m	length of the active printed monopole	13.8
W_m	width of the active printed monopole	1.8
L_p	length of the parasitic monopole	16.2
W_p	width of the parasitic monopole	3.0
L_{qw}	length of the λ/4 transformer	12.0
W_{qw}	width of the λ/4 transformer	2.3
dis	distance between the active and the parasitic elements	λ/6
gap	gap between the parasitic monopole and the grounding metal pad	0.4
via_r	radius of the platted via (through hole)	0.3

B. Simulation Results

Fig. 3 depicts the simulated reflection coefficient (S_{11}) of the printed ESPAR antenna for the two basic operating states of OFF-OFF and ON-OFF. The OFF-ON mode is not included in the simulation plot since it is identical to the ON-OFF mode (due to the design symmetry). As it is apparent from Fig. 3, both S_{11} responses exhibit a satisfying return loss (below -15 dB at 3.55 GHz) and a remarkably wide -10 dB bandwidth (both over 22%). The two corresponding radiation patterns (blue/omni – red/directive) of the antenna are plotted in Fig. 4 for the E plane (top) and the H plane (bottom). A significant 2-6 dB directivity increase can be noticed between the two operation modes, depending on which θ angle we cut the 3D pattern.

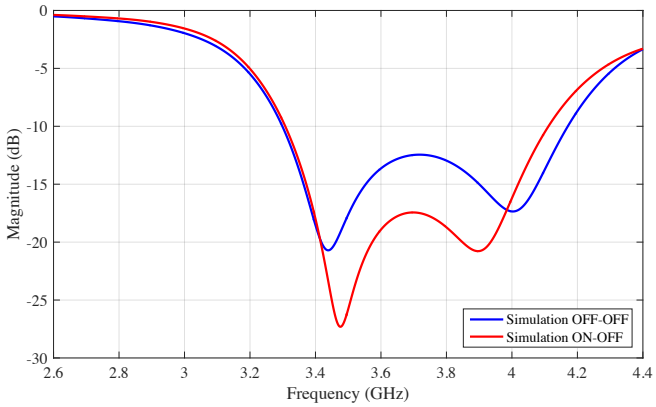

Fig. 3. Simulated reflection coefficients (S_{11}) versus frequency for the OFF-OFF and ON-OFF antenna states.

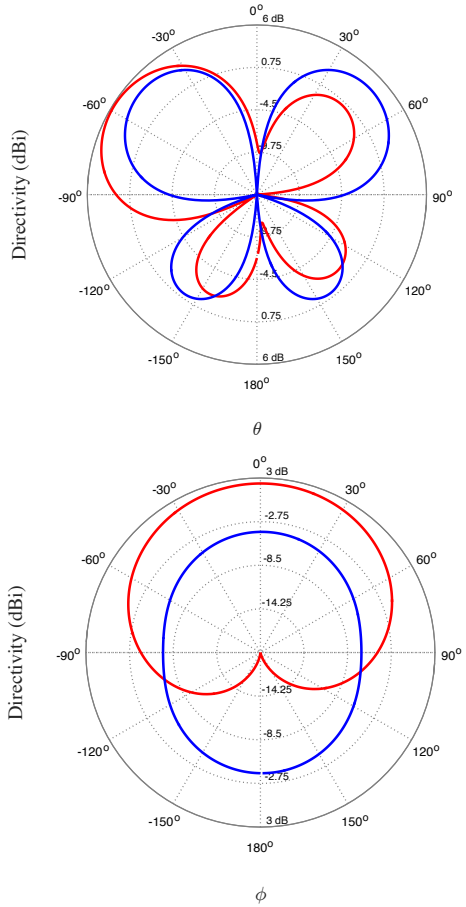

Fig. 4. The corresponding far-field 3.55 GHz directivity radiation patterns of the printed ESPAR antenna at the E plane (top) and the H plane (bottom)

III. Measurement Results of the ESPAR Antenna

Fig. 5 shows a prototype of the 3-element printed ESPAR antenna after its fabrication and assembly. All the necessary components (connector, PIN diodes, inductors, DC pins) were soldered by hand. The RF choke inductors were purchased from Coilcraft (0302CS-34NXJLU, 34 nH). The control circuit is based on the SMP1320-040LF PIN diode electronic switches manufactured by Skyworks. The simulated and the measured reflection coefficients (S_{11}) are presented in Fig. 6.

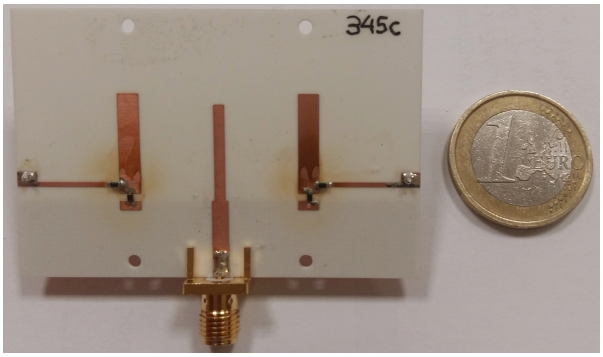

Fig. 5. The prototype printed ESPAR antenna. The close distance between the active and the parasitic elements makes the array relatively compact.

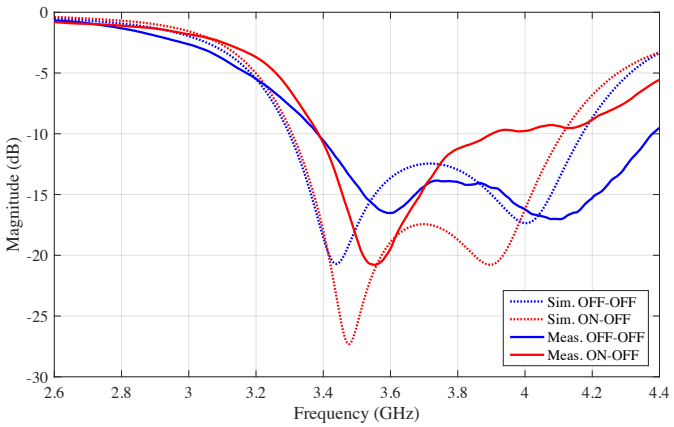

Fig. 6. The simulated and the measured reflection coefficients (S_{11}) versus frequency for the OFF-OFF and ON-OFF states of the antenna.

A slight discrepancy is observed between the simulation and the measurement results, probably due to fabrication and soldering inaccuracies. However, the measured S_{11} parameter for both states remain below -15 dB and the operating bandwidth is preserved in sufficient levels (above 14%). Figure 7 (top) contains the two corresponding measured far-field radiation patterns at the E plane for the 3.55 GHz. A considerable 5-6 dB difference between the directivities of the two states can be noticed. A small deviation at the expected upward tilt angle of the radiation is also observed. This is presumably caused by the big plastic structure that is employed in order to mount the antenna in the anechoic chamber. In Fig. 7 (bottom), the two far-field directivity patterns are plotted at the H plane. The OFF-OFF mode demonstrates a non-perfectly (quasi) omnidirectional behavior ("squeezed shape"), which is mainly induced by the planar structure of the antenna along this axis.

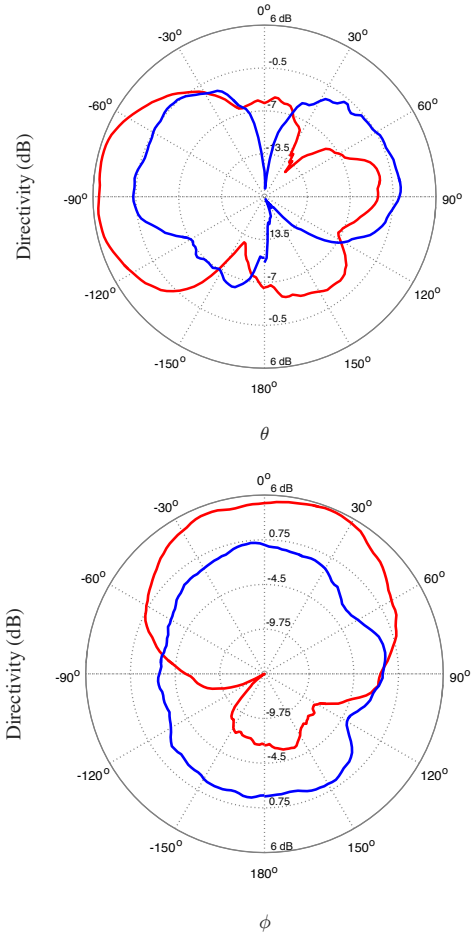

Fig. 7. The measured patterns on the E (top) and the H (bottom) plane at 3.55 GHz. The radiation pattern of the OFF-OFF is quasi-omnidirectional.

IV. System Level Experiment and Performance Evaluation

In order to validate the beam-shaping advantage of the introduced ESPAR design, a real-time over-the-air test is performed using the two prototype ESPARs with a Software Defined Radio (SDR) implementation of an IEEE 802.11p [7] Transmitter (Tx) and Receiver (Rx).

Since, the initial intention was to evaluate the antennas in vehicular systems, an in-house implementation of the IEEE 802.11p was developed. The SDR hardware that was used for digitization of the waveforms was the Universal Software Radio Peripheral (USRP) N210 [8] with SBX daughter-boards. Design (for Tx) and analysis (for Rx) of the wireless standard waveform was performed by two laptops using in-house developed software, implemented in C++. The host laptops are also connected with two single board computers. The single-board computers provide through their General Purpose Input/Output (GPIO) interface the necessary voltage in order to drive the antenna PIN diodes. The Tx transmits periodically a single signal frame every 50 msec. The IEEE

802.11p frame starts with a sequence of 10 Short Preamble Signals, where two of them are π-shifted, followed by two long preambles.

The initial Rx operations include signal detection, preamble detection and synchronization. The access medium is monitored until an incoming signal is identified by the detector. A second detector, detects IEEE 802.11p preambles and achieves synchronization based on [9]. Moreover, after synchronization, the Rx uses the preamble overhead to estimate Received Signal Strength and SNR.

A simple scenario with two portable units (Tx and Rx) is considered. Each unit is mounted on an office trolley and uses the proposed printed ESPAR reconfigurable antenna (see Fig. 8). During the evaluation test, the Tx sends a signal frame every 50msec. After Rx synchronization, signal reception and SNR estimation, the host Rx automatically sends a command to the single-board computer, in order to change the Rx pattern. For experimentation purposes, the host Rx laptop is also connected through Ethernet with the Tx single board computer. Thus, the Rx is also able to control the Tx pattern. This is an indirect way to emulate the Channel State Information feedback from Rx to Tx, that can be used for beamforming. The carrier frequency for the experiments was 3.55 GHz.

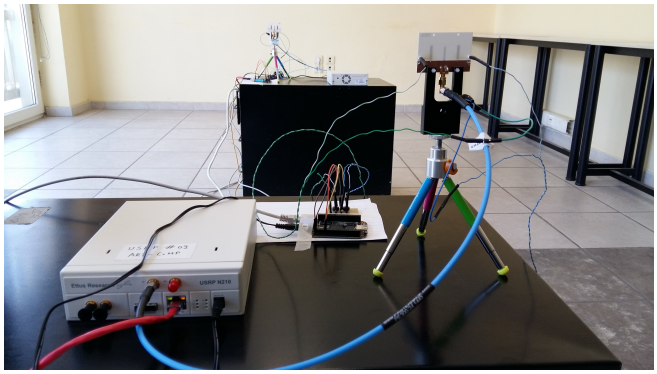

Fig. 8. The two portable units (Tx and Rx) as they were mounted on the trolleys. Each unit consists of a USRP, a single-board, a voltage divider and a prototype printed ESPAR antenna.

Tx and Rx are able to select among three patterns each: 0-0 (OFF-OFF), 1-0 (ON-OFF) and 0-1 (OFF-ON). Thus, 9 possible pattern combinations can be derived. During the experiment, the Rx spans all 9 patterns periodically and selects the combination that provides the best SNR. Fig. 9 illustrates the four different cases that are tested for the aforementioned scenario. In all four cases, the Rx remains in a fixed position. It should be noted that the planar ESPAR is always positioned in parallel with the trolley's long side orientation (see Fig. 8 for clarification). In the first case, the Tx is placed aligned at the left side of the Rx (with a 4m separation). In the second case, the Tx is moved to the opposite side of the Rx (to the right) at the same distance. At the third case, the Tx returns back to its first position but it is dis-oriented (rotated by 90°). Finally, the fourth case involves a NLOS (Non-Line of Sight) condition measurement, where the Tx is positioned out of the room.

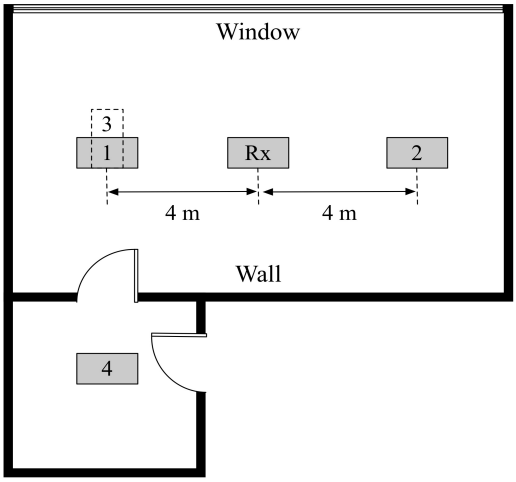

Fig. 9. The layout of the indoor test site. Rx remains stable, Tx moves in four different locations

The measurements in Positions 1 and 2 produced similar results. In the first position, 99.6% of the measurements selected pattern Tx(1,0)-Rx(0,1) as the best selection, while in position 2, 99.2% of the cases indicated pattern Tx(0,1)-Rx(1,0). In both cases, the dominant patterns were the expected ones, i.e. the combination that maximizes radiated power through the Line Of Sight (LOS) direction. In Fig. 10, the results are presented as a set of empirical Cumulative Density Functions (CDFs) of the SNR Gain of the pattern combos relative to the OMNI combination Tx(0,0)-Rx(0,0), which is denoted by the vertical red line. The superiority of the aforementioned combinations is undoubltable, providing in real channel conditions more than 6.5dB average gain for each case. The performance of combinations Tx(0,0)-Rx(0,1) and Tx(1,0)-Rx(1,0) (i.e. OMNI transmitter) is, as expected, 2-3 dB inferior. Moreover, the performance of the "opposite" pattern combos (the patterns focusing on the opposite of the LOS direction) is presented. These patterns are outperformed by the OMNI combo by more than 2.5 dB on average, while more than 10% of measurements provide gain lower than -4 dB.

In Position 3 (see Fig. 11(a)), the dominant pattern combination is Tx(0,0)-Rx(0,1), i.e. Tx is OMNI while Rx is selecting the pattern that targets Tx. However, the superiority of the pattern is not as clear as in Positions 1 and 2. Despite the fact that, it provides average gain of 4.2 dB, pattern combinations Tx(1,0)-Rx(0,1) and Tx(0,1)-Rx(0,1) were measured more suitable with higher SNR in 32% of the cases (average SNR gain 3.38, 3.9 dB respectively). Since no Tx pattern maximizes radiated power towards Tx-Rx direction, the SNR gain reduces. However, SNR gain remains relatively high for every possible Tx pattern selection. Finally, the results of Point 4 are presented in Fig.11(b). It is noted that in the NLOS scenario, there was intense mobility of scatterers in the measurement room. In this case, no dominant pattern can be identified and only 3 combinations actually outperform the OMNI combo.

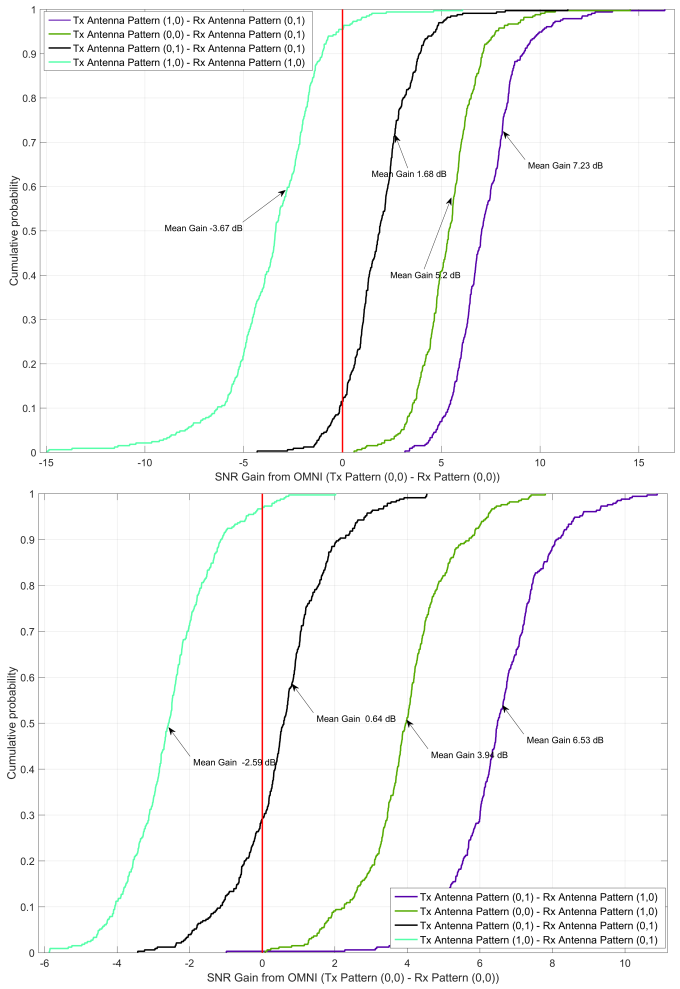

Fig. 10. Empirical CDFs of SNR gain of various pattern combinations from the OMNI combination Tx(0,0)-Rx(0,0) for (a) Points 1 and (b) 2.

However, by assuming that through the periodic measurement, the best SNR pattern combination is selected, the SNR gain (relative to the OMNI combo) is quite significant, exceeding 7.32 dB.

V. Conclusion

In this work, a new 3-printed monopole ESPAR antenna design was modelled, implemented and measured. Satisfying measured S_{11} and far-field pattern results were produced. The two developed antennas were used in an experiment designed to demonstrate their beam shaping capabilities using an SDR test-bed. Through measurements, it was demonstrated that using an SNR-based pattern selection algorithm, significant SNR gains are achieved, that exceed 6.5 dB on average.

Acknowledgment

This research has received funding from the European Union's Horizon 2020 research and innovation programme under ROADART Grant Agreement No. 636565.

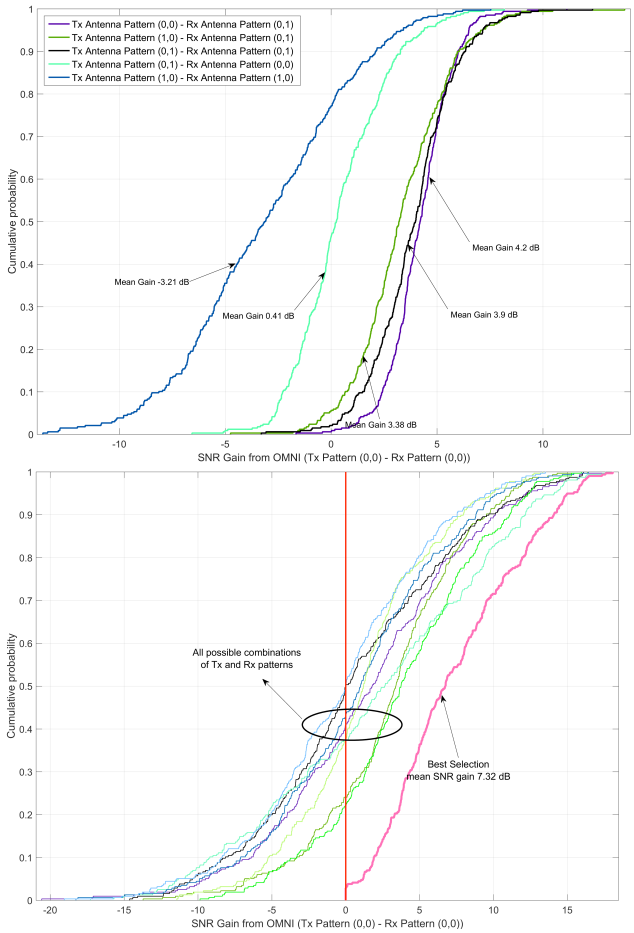

Fig. 11. Empirical CDFs of SNR gain of various pattern combinations from the OMNI combination Tx(0,0)-Rx(0,0) for (a) Points 3 and (b) 4.

References

[1] J. Lu, D. Ireland, R. Schlub, "Dielectric Embedded ESPAR (DE-ESPAR) Antenna Array for Wireless Communications," IEEE Trans. Antennas Propagat., vol. 53, no. 8, pp. 2437 – 2443, August 2005.

[2] R. Harrington, "Reactively controlled directive arrays," IEEE Trans. Antennas Propag., vol. AP-26, no. 3, pp. 390-395, May 1978.

[3] D. V. Thiel and S. L. Smith, Switched Parasitic Antennas for Cellular Communications, Norwood, MA: Artech House, 2002.

[4] T. Ohira, K. Gyoda, "Electronically steerable passive array radiator antennas for low-cost analog adaptive beamforming," in Proc. Int. Conf. Phased Array Syst. Technol., 2000, pp. 101-104.

[5] A. Kalis, A. Kanatas, C. Papadias, "A novel approach to MIMO transmission using a single RF front end," IEEE J. Sel. Areas Commun., vol. 26, no. 6, pp. 972-980. Aug. 2008.

[6] CST 3D Electromagnetic Simulation Software, www.cst.com, 2015.

[7] 802.11p-2010 - IEEE Standard for Information technology-- Local and metropolitan area networks-- Specific requirements: Wireless LAN Medium Access Control (MAC) and Physical Layer (PHY) Specifications: Wireless Access in Vehicular Environments

[8] Universal Software Radio Peripheral (USRP) Datasheet [Online]. Available: https://www.ettus.com/product/category/USRP-Networked-Series

[9] K. Shi and E. Serpedin, "Coarse frame and carrier synchronization of OFDM systems: a new metric and comparison," in IEEE Trans. Wireless Comm., vol. 3, no. 4, pp. 1271-1284, July 2004.